



SPE 105139

Fully Upscaled Saturation-Height Functions for Reservoir Modeling based on Thomeer's Method for Analyzing Capillary Pressure Measurements

Dr. J.J.M. Buiting / Saudi Aramco

Copyright 2007, Society of Petroleum Engineers

This paper was prepared for presentation at the 15th SPE Middle East Oil & Gas Show and Conference held in Bahrain International Exhibition Centre, Kingdom of Bahrain, 11–14 March 2007.

This paper was selected for presentation by an SPE Program Committee following review of information contained in an abstract submitted by the author(s). Contents of the paper, as presented, have not been reviewed by the Society of Petroleum Engineers and are subject to correction by the author(s). The material, as presented, does not necessarily reflect any position of the Society of Petroleum Engineers, its officers, or members. Papers presented at SPE meetings are subject to publication review by Editorial Committees of the Society of Petroleum Engineers. Electronic reproduction, distribution, or storage of any part of this paper for commercial purposes without the written consent of the Society of Petroleum Engineers is prohibited. Permission to reproduce in print is restricted to an abstract of not more than 300 words; illustrations may not be copied. The abstract must contain conspicuous acknowledgment of where and by whom the paper was presented. Write Librarian, SPE, P.O. Box 833836, Richardson, TX 75083-3836, U.S.A., fax 01-972-952-9435.

Abstract

Upscaling is a long standing problem for the construction of saturation height models. Upscaling is difficult when desiring to honor and retain the information obtained from core descriptions, facies classifications and mercury injection capillary pressure (MICP) data. In Saudi Aramco MICP experiments are widely used for measuring the architecture of the rock's pore system. For the analysis of these measurements Thomeer functions are standardly used. The Thomeer parameterization proved to be very adept for handling the complexity and multimodality of carbonate pore systems. In this paper a direct and closed form solution of the upscaling problem of MICP data to arbitrary large reservoir elements has been derived for standard Thomeer functions. All statistical variations of the essential rock properties, describing the architecture of the pore-system, have been included in the formalism. The upscaled result retains the familiar form of a Thomeer function while replacing single core plug values with their statistical equivalents. One of the important consequences is that intrusion of liquids for large pieces of rock can happen at much lower capillary pressures and thus much closer to the free water levels in oil reservoirs.

Introduction

Within an oil reservoir the water saturation height functions can vary strongly. In particular for carbonates these variations can be significant and difficult to estimate. The amount of hydrocarbons in a reservoir is the result of the balancing act between buoyancy- and capillary forces. Capillarity is caused by two physical phenomena, i.e. the liquid-rock interaction and the architecture of the rock's pore system. The latter

information is normally obtained through Mercury Injection Capillary Pressure (MICP) experiments on core-plugs. However, core plugs are tiny bits of rock from a specific part of the reservoir and do not represent the properties of huge piece of rock such as the grid cells in a reservoir model. Significant errors can be the result in the transition zones above the free water levels in carbonate reservoirs. The thicknesses of these zones are often underestimated when based on single or average core-plug parameters only, having significant consequences for volumetrics and production characteristics.

To calculate the saturations of large volumes of rock the full statistics of their architectural parameters have to be taken into account. For that it is required to upscale the information obtained through MICP experiments from the tiny core plug to the much larger reservoir dimensions. This upscaling has been an ongoing challenge in the oil industry for many decades.

The two best known methods to analyze MICP measurements and to estimate saturation height curves are Thomeer- and Leverett J functions. However, neither method has been satisfactorily upscaled until now. The popular J-function method usual starts with a classification of pore systems using the parameter $\sqrt{k/\phi}$. Ekran¹ has shown that saturation height data parameterized in this way do not upscale. Additional problems are encountered in carbonates with multimodal pore systems, which are better handled using the Thomeer method² for analysis of MICP measurements³.

In this paper a mathematical solution for upscaling Thomeer functions to reservoir or well log dimensions is presented. The derivations are supported by a wealth of core-plug data available in Saudi Aramco. It has been found that the final upscaled result retains the familiar form of a Thomeer function while replacing the elemental core-plug values of each specific petrophysical rock type with their statistical equivalents. In other words the statistical variations of the fundamental rock parameters within the larger rock elements play an integral part in the behavior of the upscaled saturation-height functions. As a result, hydrocarbon saturations in critical parts of the reservoirs, such as the transition zones, can be much more realistically modeled. For example, the upscaling

exercise demonstrates that transition zone thicknesses, determined from only average core-plug data, underestimate the transition zone, which could have significant effect on the estimation of the oil in place.

Some preliminary remarks:

- In this paper a solution will be derived for reservoir rock with a monomodal pore system only. It is believed that the generalization to multimodality would add additional complications to a paper that is not simple already and that it is better to leave it out of here. Carbonates, though, are in general bimodal or even trimodal. The extension to multimodality of the results as presented here is relatively straightforward.
- The distinctive shape of the Thomeer functions are the result of astute observations of Mr. Thomeer, who noted that the relation between the experimental $\log(B_v)$ values and the applied pressures $\log(P_c)$ exhibit a hyperbolic relationship. He translated this in an empirical formula, which works very well in describing MICP experiments. However, the expression has several mathematical idiosyncrasies, which made the upscaling exercise not a simple. I hope the reader bears with me.

1. The basics

From experimental data Thomeer observed hyperbolic relation between the amount of intruded mercury and the applied pressure in the log-log displays. Based on these observations he proposed an empirical relationship¹:

$$B_v(P_c) \approx \begin{cases} B_{v,\infty} \cdot \exp\left(\frac{-G}{\log(P_c) - \log(P_d)}\right) & \text{for } P_c > P_d \\ 0 & \text{elsewhere} \end{cases} \quad (1)$$

- $B_{v,\infty}$ - Fract. Bulk Vol. occupied by Hg at $P_c = \infty$
 G - Pore Geometrical Factor ($G < 2$ in general)
 P_c - Capillary pressure (applied Hg pressure)
 P_d - Minimum entry pressure

This functional form appeared to be both practical and successful. Many companies use the Thomeer parameterization for MICP experiments and for describing the internal architecture of a reservoir rock. Also in Saudi Aramco Thomeer parameters and functions are standardly used. An example of a typical Thomeer hyperbola is shown in Fig.1.

The work presented in this paper is on the upscaling of these Thomeer functions. It is also very much instigated by the issues occurring in our carbonate reservoirs, i.e. the derivations focus strongly on carbonates and it is important to remember that carbonates have in general multiple pore systems. For the sake of simplicity we treat in this paper mono-modal pore systems only. The generalization, however, to a bi- or tri-modal pore system is straightforward.

One more simplification will be introduced: for a carbonate with a mono-modal pore system it will be assumed

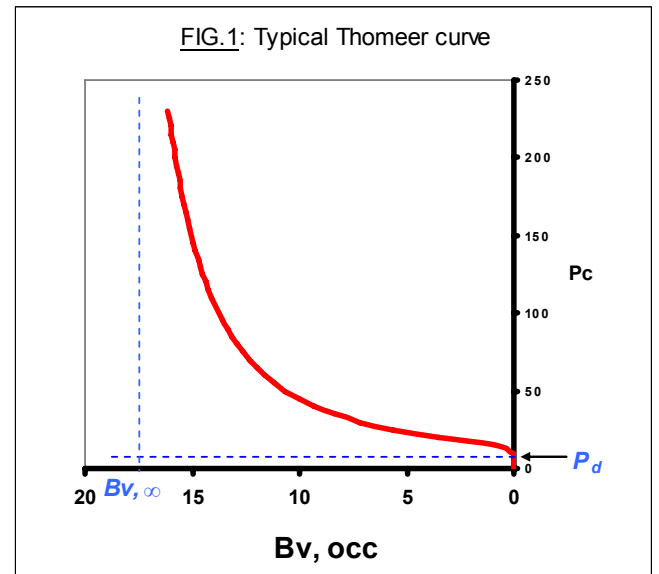
that $B_{v,\infty} \approx \phi^*$, i.e. the fractional bulk volume occupied by mercury at any P_c is than given by

$$B_v(P_c) \approx \phi \cdot \exp\left(\frac{-G}{\log(P_c) - \log(P_d)}\right) \quad \text{for } P_c > P_d \quad (2)$$

Please note that the $\exp()$ term in this equation is in fact the mercury saturation of the core-plug, i.e.

$$S_{Hg}(P_c) \approx \exp\left(\frac{-G}{\log(P_c) - \log(P_d)}\right)$$

The conversion from S_{Hg} to S_{oil} is normally done via the interfacial tension values $\sigma \cdot \cos(\theta)$ for crude, brine, rock and Hg, air, rock.



2. Q-domain representation

Even though the Thomeer parameterization is very successful and widely applied, the corresponding function – as seen in Eq.1 - has some peculiar mathematical idiosyncrasies, which are very tricky to deal with as will be seen in this paper. To being to deal with these difficulties and thus for the sake of mathematical simplicity all derivations will be done in the “Q-domain”, which is logarithmic equivalent of the pressure domain, i.e.

$$Q = \ln(P_c); \quad Q_d = \ln(P_d) \quad \text{and} \quad g = 2.3G$$

Eq.2 then obtains the form of:

$$B_v^{\phi, g, Q_d}(Q) \begin{cases} \approx \phi \cdot e^{\frac{-g}{Q - Q_d}} & \text{for } Q > Q_d \\ = 0 & \text{elsewhere} \end{cases} \quad (3)$$

In this paper it will be shown that the Thomeer hyperbolae of Eq.2, as matched against the individual MICP core plug

* This is not fully true and $B_{v,\infty}$ tends to be slightly larger than ϕ for larger bulk porosity values. Also it has to be kept in mind that we consider here a mono-modal pore system.

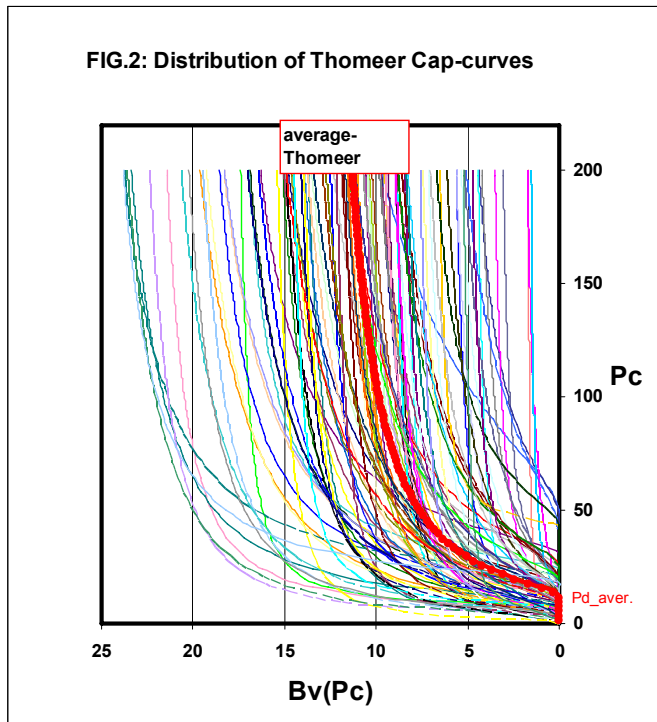
measurements can be up-scaled to larger reservoir dimensions and still retain certain relationships to the core plug Thomeer parameter distributions. This upscaled form can be written as

$$B_v^{up}(Q) \approx \bar{\phi} \cdot e^{\frac{-\bar{g}}{Q - \bar{Q}_d}},$$

which is similar to the Thomeer form, as seen in Eq.3? The plug related porosity ϕ and curvature exponent g , are replaced by their respective average values, i.e. $\bar{\phi}^*$ and \bar{g} , which are constants. The minimum-entry-pressure terms, Q_d or P_d , are replaced by \bar{Q}_d (or \bar{P}_d), which – however - is not a constant but a function of the capillary pressure Q or P_c , as will be seen later.

3. Upscaling problem

The Thomeer parameters of a tiny core plug cut out of a large piece of rock are as such not representative for its internal architecture. A typical plug has a diameter of 1.1 cm and a length of 2.54 cm, i.e. a volume of about 9.6 cm³. A reservoir rock element, such as the ones probed by wire-line logs, represents a volume sample of at least 50,000 of these core plugs in size. The dimensions of a typical grid cell in a



reservoir model is in the order of 250m x 250m x 1m, which would correspond to an equivalent of billions of core plugs and it difficult to defend that the parameters derived from a few core plugs could represent the capillary properties of such a big piece of rock.

* In principle this should read $\bar{B}_{v, \dots}$.

A large rock volume can be seen as a vast population of core plugs, each with their fundamental rock properties in terms of ϕ , G and P_d . These parameters will be distributed around their average values, valid for the rock volume. A study of over five hundred core plugs from the Ghawar Arab D limestone, on which MICP and Thomeer type curve matching was performed, has found that ϕ and G are overall normally distributed. The P_d 's exhibit a log-normal type of distribution, which implies that $Q_d = \ln(P_d)$ tend to be normally distributed[†]. Fig.2 shows a suite of Thomeer curves from a large ϕ , G , P_d distribution. Also the average Thomeer function is shown. The spread between all these functions is large.

If N is the number of plugs in a rock element, then the percentage bulk volume occupied by mercury of the upscaled rock element will be:

$$B_v^{up}(P_c) = \frac{1}{N} \sum_{i=1}^N B_{v,i}(P_c) = \bar{B}_v(P_c). \quad (4)$$

The upscaled B_v at a certain pressure P_c is determined by the averaging of the entire plug B_v 's at that P_c . Inserting the expression for of Eq.1 yields the following conditional summation:

$$B_v^{up}(P_c) = \frac{1}{N} \sum_{\substack{i=1 \\ P_{d,i} < P_c}}^N \phi_i \cdot \exp\left(\frac{-G_i}{\log(P_c) - \log(P_{d,i})}\right), \quad (5)$$

which states that only those plugs with minimum-entry-pressures P_d less than the applied pressure P_c will have been penetrated by the mercury. Using Eq.3 this expression can be simplified to:

$$B_v^{up}(Q) = \frac{1}{N} \sum_{\substack{i=1 \\ Q_{d,i} < Q}}^N \phi_i \cdot e^{\frac{-g_i}{Q - Q_{d,i}}} \quad (6)$$

This is the basic expression to be addressed, and already something can be said about its asymptotic behavior, i.e.

$$\lim_{P_c \rightarrow \infty} B_v^{up}(P_c) = \lim_{Q \rightarrow \infty} B_v^{up}(Q) = \frac{1}{N} \sum_{i=1}^N \phi_i = \bar{\phi} \quad (7a)$$

$$\lim_{B_v^{up} \rightarrow 0} P_c = P_{d, \min} \quad \text{or} \quad \lim_{B_v^{up} \rightarrow 0} Q = Q_{d, \min}. \quad (7b)$$

$Q_{d, \min}$ is related to the lowest possible minimum entry pressure, i.e. is located at the left edge of the (normal) distribution function.

Since N is large, the summation of Eq.4 can be replaced by an integral, i.e.

$$B_v^{up}(Q) = \iiint \Omega(\phi, g, Q_d) B_v^{\phi, g, Q_d}(Q) d\phi dg dQ_d \quad (8)$$

[†] For coupled normal and lognormal distributions the following relation holds: $\bar{Q}_d = \ln(P_{d, \text{median}})$.

where $\Omega(\phi, g, Q_d)$ is the 3-dimensional distribution centralized on the average position $(\bar{\phi}, \bar{g}, \bar{Q}_d)$, with the condition

$$\iiint \Omega(\phi, g, Q_d) d\phi dg dQ_d = 1 \quad (9)$$

Eq.8 is a weighted averaging of all the plugs in the rock element for a certain pressure Q (assuming that $Q > Q_{d,min}$). The result is the expectation value of all the B_v 's, which will be a certain B_v of the rock element at location $(\tilde{\phi}, \tilde{g}, \tilde{Q})$, i.e.

$$B_v^{up}(Q) = E[B_v] = B_v^{\tilde{\phi}, \tilde{g}, \tilde{Q}_d}(Q) = \tilde{\phi} \cdot e^{\frac{-\tilde{g}}{Q - \tilde{Q}_d}} \quad (10)$$

All three parameters $\tilde{\phi}$, \tilde{g} and \tilde{Q} are in principle dependent on Q (i.e. of the capillary pressure P_c) and – as indicated by the $\tilde{\sim}$ symbol - related to their respective average values. As a matter of fact $\tilde{\phi} = \bar{\phi}$ and $\tilde{g} = \bar{g}$, as will be seen later.

From the numerous carbonate measurements available it was observed that in general the correlations between ϕ , g and Q_d are weak. Only for high entry pressures G and P_d are stronger correlated, but that is only for a small portion of the core plug population.* Because of the weak inter-parameter correlations Ω can be approximated as the multiplication of the three independent centralized distributions:

$$\Omega(\phi, g, Q_d) \approx \Psi_\phi(\phi) \cdot \Psi_g(g) \cdot \Psi_{Q_d}(Q_d) \quad (11)$$

For the measured carbonates samples, it can be seen that the pore geometrical factors G 's are more-or-less normal distributed. The minimum entry pressures P_d – which are directly related to the pore-throat radii – show a skewed distribution curve, resembling a log-normal distribution. As a result, the Q_d 's are approximately normal distributed†. It is assumed that the ϕ 's are also normally distributed, but that is in fact irrelevant as will become clear later on. As a result the following normal distribution is used for all three, Q -domain, Thomeer parameters:

$$\Psi_x(x) \approx f_{\bar{x}}^\sigma(x) = \frac{1}{\sigma\sqrt{2\pi}} e^{\frac{-1}{2\sigma^2}(x-\bar{x})^2} \quad (12)$$

\bar{x} is the mean and σ the standard deviation. These are normalized Gaussians and Eq.11 can be expressed as follows:

$$\Psi(\phi, g, Q_d) \approx f_{\bar{\phi}}^{\sigma_\phi}(\phi) \cdot f_{\bar{g}}^{\sigma_g}(g) \cdot f_{\bar{Q}_d}^{\sigma_{Q_d}}(Q_d)^\ddagger \quad (13)$$

* Please note that this holds for carbonates. For clastics significant correlations do exist. The effects intra-parameter correlations will be treated in a later paper.

† Moreover it was observed that for carbonates $P_d > 1$ psi and thus that $Q_d > 0$.

‡ Note that for reasons of convenience and readability the Q_d subscript for the standard deviation σ in the above and following formulas is omitted, i.e. $\sigma \equiv \sigma_{Q_d}$

Of course normalization condition holds:

$$\iiint f_{\bar{\phi}}^{\sigma_\phi}(\phi) \cdot f_{\bar{g}}^{\sigma_g}(g) \cdot f_{\bar{Q}_d}^{\sigma_{Q_d}}(Q_d) d\phi dg dQ_d = 1 \quad (14)$$

Note that Gaussians have unlimited ranges. Practically we circumvent this by relating the standard deviation to the minimum and maximum (or low and high) values of the parameters, i.e. $\sigma \approx \frac{1}{6}(x_{max} - x_{min})$ and it is assumed that the values outside the range $[\bar{x} - 3\sigma, \bar{x} + 3\sigma]$ are negligible§. Eq.8 can then be written as:

$$B_v^{up}(Q) \approx \int_{\phi_{min}}^{\phi_{max}} \int_{g_{min}}^{g_{max}} \int_{Q_{d,min}}^Q f_{\bar{\phi}}^{\sigma_\phi}(\phi) f_{\bar{g}}^{\sigma_g}(g) f_{\bar{Q}_d}^{\sigma_{Q_d}}(Q_d) \phi e^{\frac{-g}{Q - Q_d}} d\phi dg dQ_d \quad (15)$$

This is the basic integral to be solved.

4. The ϕ -integral

The porosity part of the integral can be taken outside the combined integration:

$$B_v^{up}(Q) \approx \int_{\phi_{min}}^{\phi_{max}} \underbrace{f_{\bar{\phi}}^{\sigma_\phi}(\phi) d\phi}_{=\tilde{\phi}} \int_{g_{min}}^{g_{max}} \int_{Q_{d,min}}^Q f_{\bar{g}}^{\sigma_g}(g) f_{\bar{Q}_d}^{\sigma_{Q_d}}(Q_d) e^{\frac{-g}{Q - Q_d}} dg dQ_d \quad (16)$$

or

$$B_v^{up}(Q) \approx \tilde{\phi} \int_{g_{min}}^{g_{max}} \int_{Q_{d,min}}^Q f_{\bar{g}}^{\sigma_g}(g) f_{\bar{Q}_d}^{\sigma_{Q_d}}(Q_d) e^{\frac{-g}{Q - Q_d}} dg dQ_d \quad (17)$$

This resolves the ϕ (or $B_{v,\infty}$) contribution to integral Eq.15. The averaged result as expressed in Eq.10 can be written as:

$$B_v^{up}(Q) = B_v^{\bar{\phi}, \bar{g}, \bar{Q}_d}(Q) = \bar{\phi} \cdot e^{\frac{-\bar{g}}{Q - \bar{Q}_d}}, \quad i.e. \quad \tilde{\phi} = \bar{\phi} \quad (18)$$

Moreover, the up-scaled B_v is independent** of the variation in porosity, i.e. $\sigma_\phi \dots$ Note that the above result is valid for any shape of the porosity distribution.

5. The g -integral

Rearranging the terms in Eq.17 yields

$$B_v^{up}(Q) \approx \bar{\phi} \int_{Q_{d,min}}^Q f_{\bar{Q}_d}^{\sigma_{Q_d}}(Q_d) \left[\int_{g_{min}}^{g_{max}} f_{\bar{g}}^{\sigma_g}(g) \cdot e^{\frac{-g}{Q - Q_d}} dg \right] dQ_d \quad (19)$$

Here we introduce another simplification by removing the ϕ

§ About 1% of the Gaussian distribution falls outside the range.

** For weak correlations between the parameters!

contribution altogether for the time being, i.e.

$$b_v^{up}(Q) \equiv \frac{B_v^{up}(Q)}{\phi} = e^{-\frac{\bar{g}}{Q-Q_d}} \quad (Q > Q_{d,min}) \quad (20)^*$$

The integral of Eq.19 then becomes:

$$b_v^{up}(Q) \approx \int_{Q_{d,min}}^Q f_{Q_d}^{\sigma_g}(Q_d) \left[\int_{g_{min}}^{g_{max}} f_g^{\sigma_g}(g) e^{-\frac{g}{Q-Q_d}} dg \right] dQ_d \quad (21)$$

The first integral in Eq.21 to tackle is the g -integral:

$$I_g = \int_{g_{min}}^{g_{max}} f_g^{\sigma_g}(g) e^{-\frac{g}{Q-Q_d}} dg = \int_{g_{min}}^{g_{max}} \frac{1}{\sigma_g \sqrt{2\pi}} e^{-\frac{(g-\bar{g})^2}{2\sigma_g^2}} e^{-\frac{g}{Q-Q_d}} dg \quad (22)$$

After some rearranging this can be rewritten as:

$$I_g = e^{\frac{-\bar{g}}{(Q-Q_d)} + \frac{\sigma_g^2}{2(Q-Q_d)^2}} \underbrace{\int_{g_{min}}^{g_{max}} \frac{1}{\sigma_g \sqrt{2\pi}} e^{-\frac{1}{2\sigma_g^2} \left\{ g - \bar{g} + \frac{\sigma_g^2}{(Q-Q_d)} \right\}^2} dg}_{=\Lambda_{\bar{g}'}^{\sigma_g}(g_{max}) - \Lambda_{\bar{g}'}^{\sigma_g}(g_{min}), \text{ where } \bar{g}' = \bar{g} + \frac{\sigma_g^2}{(Q-Q_d)}}$$

This converts the I_g integral into:

$$I_g = e^{\frac{-\bar{g}}{(Q-Q_d)} + \frac{\sigma_g^2}{2(Q-Q_d)^2}} \left\{ \Lambda_{\bar{g}'}^{\sigma_g}(g_{max}) - \Lambda_{\bar{g}'}^{\sigma_g}(g_{min}) \right\} \quad (23)$$

Where $\Lambda_x^{\sigma}(x)$ is the probability function defined as

$$\Lambda_x^{\sigma}(x) = \frac{1}{\sigma \sqrt{2\pi}} \int_{-\infty}^{x'-x} e^{-\frac{(x'-x)^2}{2\sigma^2}} dx' \quad (24)$$

The individual components are displayed in Fig.3.

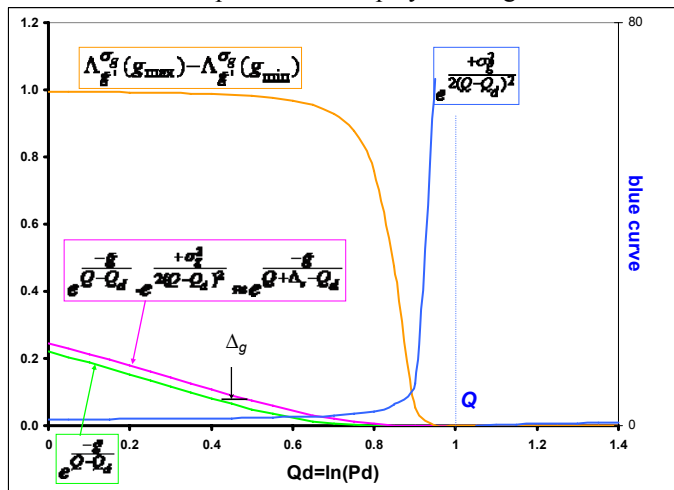


Fig.3: The components contributing to the g integration. The multiplication by the positive and singular exponential (blue curve) causes a shift Δ_g in the Q -domain.

* This actually is the Hg-saturation, i.e. $S_{Hg}(Q) = \exp\left(\frac{-\bar{g}}{Q-Q_d}\right)$ in case of a mono-modal system and $B_{v,-} \approx \phi$.

Note that $\lim_{Q_d \rightarrow Q} e^{\frac{\sigma_g^2}{2(Q-Q_d)^2}} = \infty$, i.e. this exponential is divergent,

but also observe that this singularity is annihilated by the second term in Eq.23, i.e.

$$\Lambda_{\bar{g}'}^{\sigma_g}(g_{max}) - \Lambda_{\bar{g}'}^{\sigma_g}(g_{min}) \begin{cases} \approx 1 & \text{for } Q_d < Q - \frac{\sigma_g}{3} \\ \approx 0 & \text{for } Q - \frac{\sigma_g}{3} < Q_d < Q \end{cases}$$

where $\bar{g}' = \bar{g} + \frac{\sigma_g^2}{(Q-Q_d)}$!

With this observation Eq. 23 can be expressed as:

$$I_g \approx \begin{cases} e^{\frac{-\bar{g}}{(Q-Q_d)} + \frac{\sigma_g^2}{2(Q-Q_d)^2}} & \text{for } Q_d < Q - \frac{\sigma_g}{3} \\ 0 & \text{for } Q - \frac{\sigma_g}{3} < Q_d < Q \end{cases} \quad (25)$$

For $Q_d < Q - \frac{\sigma_g}{3}$ the $e^{\frac{\sigma_g^2}{2(Q-Q_d)^2}}$ term is well behaved and, in essence, introduces only a small, constant shift Δ_g in the Q -domain as can be seen in Fig.3.

This shift can be estimated for $Q_d < Q - \frac{\sigma_g}{2\bar{g}}$ (which holds

since $Q_d < Q - \frac{\sigma_g}{3}$ and $\bar{g} \approx 3\sigma_g$) as follows:

$$e^{\frac{-\bar{g}}{(Q-Q_d)} + \frac{\sigma_g^2}{2(Q-Q_d)^2}} = e^{\frac{-\bar{g}}{(Q-Q_d)} \left\{ 1 - \frac{\sigma_g^2}{2\bar{g}(Q-Q_d)} \right\}} = e^{\frac{-\bar{g}}{(Q-Q_d)} \left\{ 1 - \sigma_g^2 / 2\bar{g}(Q-Q_d) \right\}} \quad (26)$$

Since $\sigma_g^2 / 2\bar{g}(Q-Q_d) \ll 1$ the above equation can be approximated as:

$$e^{\frac{-\bar{g}}{(Q-Q_d)} + \frac{\sigma_g^2}{2(Q-Q_d)^2}} \approx e^{\frac{-\bar{g}}{(Q-Q_d)} \frac{1}{1 + \sigma_g^2 / 2\bar{g}(Q-Q_d)}} \quad \text{or} \\ e^{\frac{-\bar{g}}{(Q-Q_d)} + \frac{\sigma_g^2}{2(Q-Q_d)^2}} \approx e^{-\bar{g} / \left(Q + \frac{\sigma_g^2}{2\bar{g}} - Q_d \right)} = e^{\frac{-\bar{g}}{Q + \Delta_g - Q_d}} \quad (27)$$

From which follows that: $\Delta_g \approx \frac{\sigma_g^2}{2\bar{g}}$ (28)[†]

Since $\Delta_g > 0$ and $Q_d < Q$, the integral I_g of Eq.25 can be expressed as:

$$I_g \approx \begin{cases} e^{\frac{-\bar{g}}{(Q+\Delta_g-Q_d)}} & \text{for } Q_d < Q \\ 0 & \text{elsewhere} \end{cases} \quad (29)$$

So in conclusion, the upscaling step in the g -domain reduces the distribution of g 's to its average value, i.e. $\tilde{g} = \bar{g}$, and, as

[†] A typical value is $\Delta_g \approx 0.07$.

an additional effect, introduces a small and positive shift in the Q -domain, i.e. $Q \rightarrow Q + \Delta_g$ *. As a result Eqs.10 and 18 evolve into:

$$B_v^{up}(Q) = B_v^{\bar{\phi}, \bar{g}, \bar{Q}_d}(Q) = \bar{\phi} \cdot e^{\frac{-\bar{g}}{Q + \Delta_g - \bar{Q}_d}} \quad (30)$$

So in effect $\tilde{\phi} = \bar{\phi}$ and $\tilde{g} = \bar{g}$, with the caveat that the variation in the g -domain, i.e. σ_g , remains a factor through the shift Δ_g in the Q -domain.

6. The Q_d integral: preliminaries

Through the result of Eq.29, the integral of Eq.21 reduces to:

$$b_v^{up}(Q) \approx \int_{Q_{d,min}}^Q f_{\bar{Q}_d}^\sigma(Q_d) e^{\frac{-\bar{g}}{(Q + \Delta_g - Q_d)}} dQ_d \quad (31)$$

Since $f_{\bar{Q}_d}^\sigma(Q_d) \approx 0$ for $Q_d < Q_{d,min}$, the lower range of this integral can be extended from $Q_{d,min}$ down to $-\infty^\dagger$, i.e.

$$b_v^{up}(Q) \approx \int_{-\infty}^Q f_{\bar{Q}_d}^\sigma(Q_d) e^{\frac{-\bar{g}}{(Q + \Delta_g - Q_d)}} dQ_d$$

or

$$b_v^{up}(Q) \approx \frac{1}{\sigma\sqrt{2\pi}} \int_{-\infty}^Q e^{\frac{-\bar{g}}{(Q + \Delta_g - Q_d)}} e^{-\frac{(Q_d - \bar{Q}_d)^2}{2\sigma^2}} dQ_d \quad (32)$$

The behavior of the two exponential functions in Q_d -domain is displayed in Fig.4a, keeping in mind that the Thomeer function are zero for $Q_d > Q$. The combination of the exponentials is shown in Fig.4b and the integral of Eq.32 represents in effect the areas under the distorted bell curves as seen in Fig.4b.

Eq.32 is in fact the weighted average of $e^{\frac{-\bar{g}}{(Q + \Delta_g - Q_d)}}$ and therefore

$$b_v^{up}(Q) \approx e^{\frac{-\bar{g}}{(Q + \Delta_g - \bar{Q}_d)}} \quad (33)$$

where $Q_{d,min} < \bar{Q}_d < Q$.

There are two difficulties with integral Eq.33. Firstly its range is limited to $Q_d \leq Q$. In other words, only plugs with a minimum entry pressures P_d less than the applied pressure P_c are being filled with mercury and contribute to the total amount of liquid in the rock element. Secondly the function has a singularity at $Q_d = Q + \Delta_g$ and even though the integration does not reach that far, the integral is improper and

no straightforward indefinite solution is available[‡]. To circumvent this problem some pragmatic approximations had to be found.

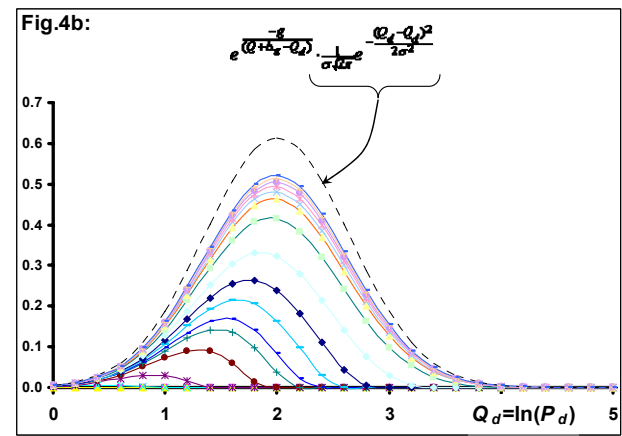
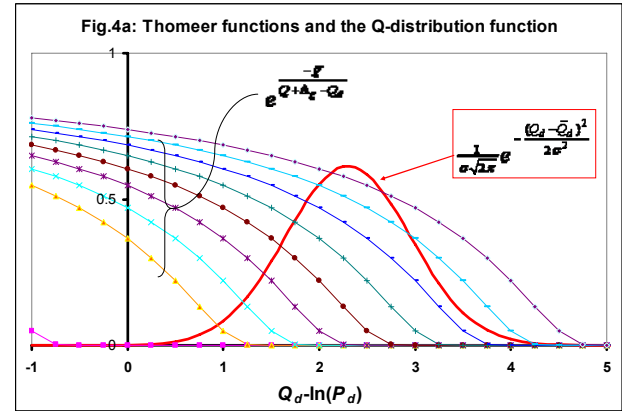


Fig.4: Comparing the individual components comprising the integral of Eq.32 in Fig.4a and the effect of the multiplication in Fig.4b. The multiplication results in distorted bell curves. The original normal distribution of the Q_d 's is shown as a dashed curve, enveloping all the other ones. The integrals of Eq.32 represent the areas under the distorted bell curves of Fig.4b and are well behaved, disregarding the impropriety of the Thomeer function.

6.1 Solving via a coordinate transformation

Because of the impropriety of the integral of Eq.33 a pragmatic solution will be derived by proxy. To achieve this coordinate transformation centered around the point $Q + \Delta_g$ is introduced:

$$\begin{aligned} y &= \frac{1}{\sigma_g}(Q + \Delta_g - Q_d) && \text{- related to min. entry press.} \\ \bar{y} &= \frac{1}{\sigma_g}(Q + \Delta_g - \bar{Q}_d) && \text{- related to aver. min. entry press.} \\ \tilde{y} &= \frac{1}{\sigma_g}(Q + \Delta_g - \tilde{Q}_d) && \text{- the upscaled version} \\ y_o &= \frac{1}{\sigma_g}(Q + \Delta_g - Q_o) && \text{- for later usage} \end{aligned} \quad (34)$$

* Or a negative shift in the Q_d -domain: , i.e. $Q_d \rightarrow Q_d - \Delta_g$.

† For carbonates in general $P_d > 1$ psi, i.e. $Q_d > 0$.

‡ However since the roots are outside the integration limits (Δ_g is a positive number) a finite value exists, as can be concluded from Fig. 4b as well.

Moreover, $\delta_y = \frac{\Delta_g}{\bar{g}} \quad (= \frac{\sigma_g^2}{2\bar{g}^2} > 0)$ and $\sigma_y = \frac{\sigma}{\bar{g}}$.

Note that since the pore geometrical factors G (and thus g) are normally distributed and positive by definition, the maximum size of its standard deviation is limited by the value of its average value, i.e. $\sigma_g \leq \frac{1}{3}\bar{g} \rightarrow \delta_y \leq \frac{1}{18}$. Moreover $Q > Q_d$ or $y > \delta_y^*$ and Eq.32 can be expressed in the y -domain as:

$$b_v^{mp}(Q) = \frac{1}{\sigma_y \sqrt{2\pi}} \int_{\delta_y}^{\infty} e^{-\frac{1}{y}} e^{-\frac{(y-\bar{y})^2}{2\sigma_y^2}} dy \quad (35)$$

Introducing the function $\beta(y) = e^{-\frac{1}{y}}$ for $y > 0$ and $\beta(y \leq 0) = 0$, Eq.35 expressed in terms of this $\beta(y)$ becomes:

$$b_v^{mp}(Q) = \frac{1}{\sigma_y \sqrt{2\pi}} \int_{\delta_y}^{\infty} \beta(y) e^{-\frac{(y-\bar{y})^2}{2\sigma_y^2}} dy \equiv I_y \quad (36)$$

Some of the properties of this function are summarized in the Appendix. Note that $\beta(y)$ is analogous to Eq.20. Moreover since $0 < \delta_y < 0.06$, and thus small, $\beta(0 < y < \delta_y) \approx 0$ for all practical purposes and it is possible to extend the lower limit of the above integral to 0.

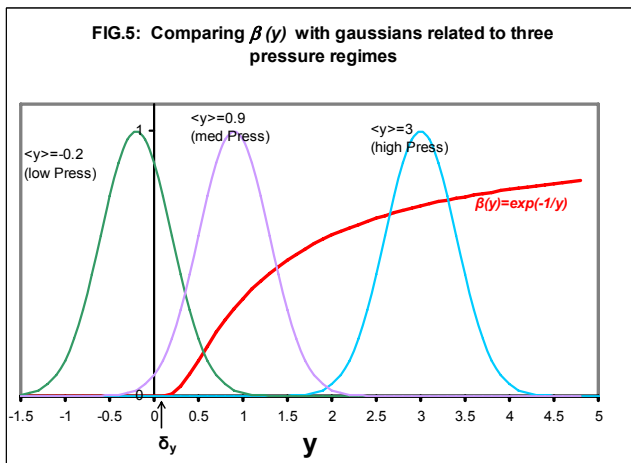


Fig.5: The $\beta(y)$ function and 3 normal distributions related to different pressure regimes. Only the high pressure curve falls within range of $y > \delta_y$. The other two only have partial coverage of $\beta(y)$ and the integral I_y is more difficult.

In Fig.5 $\beta(y)$ and three normal distributions are shown, each related to a different pressure[†]. For the high pressure case the Gaussian covers a small, almost linear part of the $\beta(y)$ -curve and the resulting mean value $\beta(\tilde{y}) \approx \beta(\bar{y})$. In the low pressure case, only values between ≈ 0.2 and 1.0 contribute to the integral of Eq.36.

* Note that even though y is always positive, \bar{y} can be negative.

† Here it needs to be noted that the values of the \bar{y} 's not only depend on the pressures Q and Q_d , but also on the values of the g 's (Eq.34), i.e. high \bar{y} values can also be a sign of an abnormal low \bar{g} value.

6.2 High pressure solution

For large values of the applied mercury pressures, i.e. P_c 's above the highest possible minimum entry pressures $P_{d,max}$, all elemental rock elements (core-plug equivalents) are being intruded by mercury. This implies that $P_c > P_{d,max}$ and thus $Q > \bar{Q}_{d,max} \approx \bar{Q}_d + 3\sigma$. In terms of the y 's this means (see Eq.34) that

$$\bar{y} > 3\sigma_y + \delta_y \quad (37)$$

and that the range of the Gaussians or bell curves fall totally within the validity range of $\beta(y)$, i.e. $y > 0$, as can be seen by Fig.5. Note that by definition $\beta(y < 0) = 0$. Moreover, $\beta(0 < y < \delta_y) \approx 0$ – as is also explained in the Appendix – and that therefore the lower integration limit of Eq.36 can be extended from δ_y to $-\infty$, i.e.

$$I_{\bar{y}} = \frac{1}{\sigma_y \sqrt{2\pi}} \int_{-\infty}^{\infty} \beta(y) e^{-\frac{(y-\bar{y})^2}{2\sigma_y^2}} dy = E[\beta] = \bar{\beta} \quad (38)$$

This extension has the advantage that the standard definitions for the statistical parameters of a normal distribution such as mean and variance can be employed. In particular for functions which vary slowly compared to the standard deviation, such as is the case for the high pressure bell curve in Fig.5, where the β -function is more-or-less linear over the range of the bell-curve. In these cases the β -function in the vicinity of \bar{y} can be approximated by a Taylor expansion

$$\beta(y) \approx \beta(\bar{y}) + (y - \bar{y})\beta'(\bar{y}) + \frac{1}{2}(y - \bar{y})^2\beta''(\bar{y})$$

yielding the following result for the integral:

$$\frac{1}{\sigma_y \sqrt{2\pi}} \int_{-\infty}^{\infty} \beta(y) e^{-\frac{(y-\bar{y})^2}{2\sigma_y^2}} dy \approx \beta(\bar{y}) + \frac{1}{2}\sigma_y^2 \cdot \beta''(\bar{y}) \quad (39)$$

$$\text{where } \beta''(\bar{y}) = \frac{\partial^2 \beta}{\partial y^2} \Big|_{y=\bar{y}} = \beta(\bar{y}) \left(\frac{1}{\bar{y}^4} - \frac{2}{\bar{y}^3} \right) \quad (40)$$

and thus

$$I_{\bar{y}} \approx \beta(\bar{y}) \left[1 + \frac{\sigma_y^2}{2} \cdot \left(\frac{1}{\bar{y}^4} - \frac{2}{\bar{y}^3} \right) \right] \quad \text{for } \bar{y} > 3\sigma_y + \delta_y \quad (41)$$

Since $\beta(y)$ varies slowly for high y values the I_y is the expectation or mean value of the population of the β 's. The result should be a β -value closely located to the average of the parameter y , i.e. \bar{y} :

$$I_{\bar{y}} = E[\beta] = \exp\left(\frac{-1}{\bar{y} + \delta_{hp}}\right) = \beta(\tilde{y}), \quad \text{where } \tilde{y} = \bar{y} + \delta_{hp} \quad (42)$$

For small δ_{hp} a Taylor expansion can be applied:

$$\beta(\bar{y} + \delta_{hp}) \approx \beta(\bar{y}) + \delta_{hp} \cdot \beta'(\bar{y}) = \beta(\bar{y}) \cdot \left(1 + \frac{\delta_{hp}}{\bar{y}^2}\right) \quad (43)$$

Combining these results with Eq.41 yields:

$$\beta(\bar{y}) \cdot \left[1 + \frac{\sigma_y^2}{2} \cdot \left(\frac{1}{\bar{y}^4} - \frac{2}{\bar{y}^3}\right)\right] \approx \beta(\bar{y}) \left(1 + \frac{\delta_{hp}}{\bar{y}^2}\right) \quad (44)$$

From this equation δ_{hp} can be solved, i.e.

$$\delta_{hp} \approx \frac{\sigma_y^2}{2} \cdot \left(\frac{1}{\bar{y}^2} - \frac{2}{\bar{y}}\right) \text{ for } \bar{y} > 3\sigma_y + \delta_y \quad (45)$$

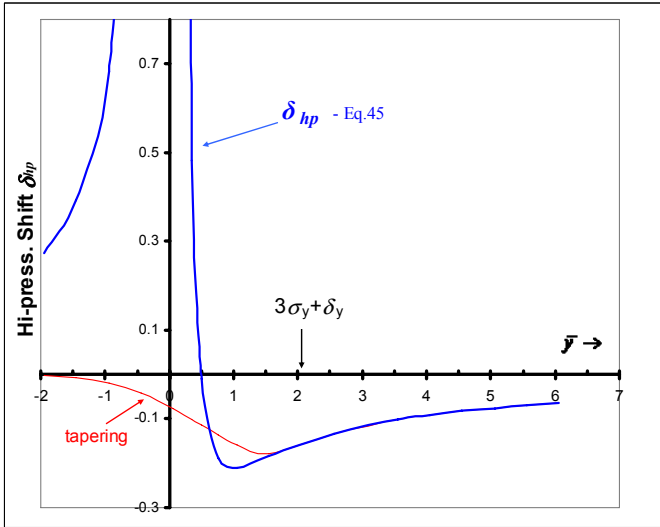


Fig.6: The high pressure shift δ_{hp} of Eq.45. For high pressures, i.e. beyond the point $3\sigma_y + \delta_y$ the shift is a slowly varying negative number. Before that point the function becomes anomalous. To avoid this behavior a tapering can be applied as is shown by the red curve.

The behavior of δ_{hp} as function of \bar{y} can be seen in Fig.6. Note that $\delta_{hp}=0$ for $\bar{y} = \frac{1}{2}$ and becoming singular at $\bar{y} = 0$. Within the validity range for high pressures, i.e. for $\bar{y} > 3\sigma_y + \delta_y$ (see Eq.37) the shift δ_{hp} is negative and slowly approaching 0 in an almost linear fashion. This shift results from the second-derivative of β (Eq.39), yielding the variance dependency as seen in Eq.45. It will be used later on. For smaller values of \bar{y} the δ_{hp} function of Eq.45 is not well behaved. In these cases the high \bar{y} assumptions, embedded in Eqs. 38 and 39, are not valid anymore. In Fig.6 a tapering (red curve) is applied for those values. The reasons will be explained below.

With the expression for the δ_{hp} shift, valid for high \bar{y} values, the high pressure (and/or low \bar{g}) case of the upscaling problem has been solved. From Eq.42 it is known that $\tilde{y} = \bar{y} + \delta_{hp}$. Using the coordinate transformations of Eq.34 the upscaled (log) minimum entry pressure function \tilde{Q}_d can be written as $\tilde{Q}_d = \bar{Q}_d + \Delta_{hp}$. Here $\Delta_{hp} = -\bar{g}\delta_{hp}$, which is a positive number for the high pressure regions. Substituting this into the intermediate result of Eq.30, yields the high pressure solution:

$$B_v^{up}(Q) = \bar{\phi} \exp\left[\frac{-\bar{g}}{Q + \Delta_g - \bar{Q}_d - \Delta_{hp}}\right], \quad (46)$$

As mentioned: $\Delta_{hp} = -\bar{g}\delta_{hp}$ and is positive and well behaved for high pressures and/or low \bar{g} values, i.e. in the region where $\bar{y} > 3\sigma_y + \delta_y$ in Fig.6. From Fig.6 it can also be seen that this shift becomes anomalous for low \bar{y} values. To avoid this problem a low- \bar{y} tapering is introduced, as already indicated in Fig.6. This results in the following high-pressure shift function in the Q -domain, which is positive for all values of Q and has no effect for low Q -values:

$$\Delta_{hp} \approx \begin{cases} \frac{\sigma^2}{w} \left(1 - \frac{\bar{g}}{2w}\right) & \text{for } w \geq w_o \\ \frac{\sigma^2}{w_o} \left(1 - \frac{\bar{g}}{2w_o}\right) \exp\left(\frac{-1}{2\sigma_{hp}^2} (w - w_o)^2\right) & \text{for } w < w_o \end{cases} \quad (47)$$

where

$$\begin{aligned} w &= Q - \bar{Q}_d + \Delta_g \\ w_o &= \sigma + \bar{g} \\ \sigma_{hp} &\approx \frac{1}{3}(\bar{Q}_d + \sigma + \bar{g}) \end{aligned}$$

The parameters w_o and σ_{hp} are chosen in such way to assure proper tapering to the low Q -side and sufficient shifting effects for the higher Q -values. This function is shown in Fig.7 for several values of the average (log) minimum entry pressures and average pore geometrical factors, i.e. several (\bar{Q}_d, \bar{g}) combinations.

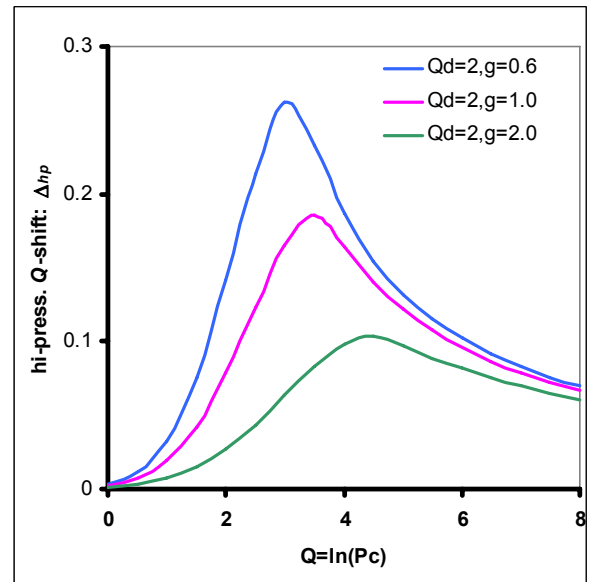


Fig.7: Examples of the high pressure shift function Δ_{hp} as defined by Eq.47 for three different combination of (\bar{Q}_d, \bar{g}) . Note the low Q tapering. For high Q 's the shift goes to zero.

6.3 Low to medium pressure regime

For $Q < \bar{Q}_d + 3\sigma = Q_{d,\max}$, the integration over Q_d , and thus over y (Eq.36), can not be extended anymore over the range $-\infty \rightarrow +\infty$ and a different approach to solve the integral is needed. Again the problem will be tackled using the y -transformation defined by Eqs.34 and 35, i.e. by solving:

$$I_{\bar{y}} = \frac{1}{\sigma_y \sqrt{2\pi}} \int_{\delta_y}^{\infty} e^{-\frac{1}{y}} e^{-\frac{(y-\bar{y})^2}{2\sigma_y^2}} dy = \beta(\bar{y}) \quad (48)$$

A graphical representation of the contributing functions is shown in Fig.5, but now we concentrate on the bell curves related to the low- and medium pressures.

As argued before, Eq.48 yields an average value of the β 's with respect to a normally distributed y 's:

$$I_{\bar{y}} = \frac{1}{\sigma_y \sqrt{2\pi}} \int_{\delta_y}^{\infty} \beta(y) e^{-\frac{(y-\bar{y})^2}{2\sigma_y^2}} dy = \bar{\beta} = \beta(\bar{y}) \quad (49)$$

where \bar{y} is assumed to be somewhere between δ_y and $y+3\sigma_y$. The objective is to find an accurate estimate of this \bar{y} . This is achieved by using the fact that for smaller y 's, and for the purpose of finding a good \bar{y} , a linear approximation is made, i.e.

$$\beta(y) = \begin{cases} e^{-\frac{1}{y}} \approx \alpha(y - y_o) & \text{for } y_o < y < \bar{y} + 3\sigma_y \\ 0 & \text{for } y < y_o \end{cases} \quad (50)$$

The line $\alpha(y-y_o)$ passes to the inflection point of the β -function at $y = \frac{1}{2}$, where $\beta'(y)$ is at its maximum and thus $\beta''(\frac{1}{2}) = 0$. Then the slope $\alpha = \beta'(\frac{1}{2}) = 0.54$ and it intercepts the y -axis at $y_o = \frac{1}{4}$. See also the Appendix. Substituting the linear approximation in Eq.49 yields:

$$\frac{1}{\sigma_y \sqrt{2\pi}} \int_{y_o}^{\infty} \alpha(y - y_o) e^{-\frac{(y-\bar{y})^2}{2\sigma_y^2}} dy \approx \alpha(\bar{y} - y_o) \quad (51)$$

From which \bar{y} can be solved, with the understanding that it is good for those y ranges where the linear approximation yields a \bar{y} comparable to the one we would get by solving Eq.49 for $\beta(y)$. This works amazingly well for the medium pressure cases, but some adjustments are needed for the very low pressures and of course for the high pressures.

Note that the slope α drops out of eq.51 and we get:

$$\bar{y} \approx y_o - y_o \frac{1}{\sigma_y \sqrt{2\pi}} \int_{y_o}^{\infty} e^{-\frac{(y-\bar{y})^2}{2\sigma_y^2}} dy + \frac{1}{\sigma_y \sqrt{2\pi}} \int_{y_o}^{\infty} y e^{-\frac{(y-\bar{y})^2}{2\sigma_y^2}} dy$$

By replacing y in the second integral with $(y - \bar{y}) + \bar{y}$ one obtains:

$$\begin{aligned} \bar{y} &\approx y_o - y_o \frac{1}{\sigma_y \sqrt{2\pi}} \int_{y_o}^{\infty} e^{-\frac{(y-\bar{y})^2}{2\sigma_y^2}} dy \\ &+ \bar{y} \frac{1}{\sigma_y \sqrt{2\pi}} \int_{y_o}^{\infty} e^{-\frac{(y-\bar{y})^2}{2\sigma_y^2}} dy \\ &+ \frac{1}{\sigma_y \sqrt{2\pi}} \int_{y=y_o}^{\infty} (y - \bar{y}) e^{-\frac{(y-\bar{y})^2}{2\sigma_y^2}} dy \end{aligned} \quad (52)$$

The first two integrals are complementary probability functions (compare to Eq.24). The 3rd integral can be solved by changing the integration variable from y to $(y - \bar{y})$, i.e.

$$\begin{aligned} \bar{y} &\approx y_o - y_o \left[1 - \Lambda_{\bar{y}}^{\sigma_y}(y_o) \right] + \bar{y} \left[1 - \Lambda_{\bar{y}}^{\sigma_y}(y_o) \right] \\ &+ \frac{1}{\sigma_y \sqrt{2\pi}} \int_{y-\bar{y}=y_o-\bar{y}}^{\infty} (y - \bar{y}) e^{-\frac{(y-\bar{y})^2}{2\sigma_y^2}} d(y - \bar{y}) \end{aligned}$$

where Λ is the probability function (see Eq.24). Note that the expression $[1-\Lambda]$ is equivalent to the complementary probability function.

Further rearrangements lead to:

$$\bar{y} \approx y_o \cdot \Lambda_{\bar{y}}^{\sigma_y}(y_o) + \bar{y} \left[1 - \Lambda_{\bar{y}}^{\sigma_y}(y_o) \right] + \frac{1}{\sigma_y \sqrt{2\pi}} \int_{z=y_o-\bar{y}}^{\infty} \frac{1}{2} e^{-\frac{z^2}{2\sigma_y^2}} dz^2$$

By substituting $u = \frac{z^2}{2\sigma_y^2}$ one gets

$$\bar{y} \approx y_o \cdot \Lambda_{\bar{y}}^{\sigma_y}(y_o) + \bar{y} \left[1 - \Lambda_{\bar{y}}^{\sigma_y}(y_o) \right] + \frac{2\sigma_y^2}{2} \frac{1}{\sigma_y \sqrt{2\pi}} \int_{u=\frac{(y_o-\bar{y})^2}{2\sigma_y^2}}^{\infty} e^{-u} du$$

And thus

$$\bar{y} \approx y_o \cdot \Lambda_{\bar{y}}^{\sigma_y}(y_o) + \bar{y} \left[1 - \Lambda_{\bar{y}}^{\sigma_y}(y_o) \right] + \sigma_y^2 \frac{1}{\sigma_y \sqrt{2\pi}} e^{-\frac{(y_o-\bar{y})^2}{2\sigma_y^2}}$$

and via Eq.12:

$$\bar{y} \approx y_o \cdot \Lambda_{\bar{y}}^{\sigma_y}(y_o) + \bar{y} \left[1 - \Lambda_{\bar{y}}^{\sigma_y}(y_o) \right] + \sigma_y^2 \cdot f_{\bar{y}}^{\sigma_y}(y_o) \quad (53)$$

In general $\Lambda_{\bar{x}}^{\sigma}(x) = \Lambda_0^{\sigma}(x - \bar{x})$ and $f_{\bar{x}}^{\sigma}(x) = f_0^{\sigma}(x - \bar{x})$ and Eq.53 can be written as (omitting the "0"-subscripts):

$$\bar{y} \approx y_o \cdot \Lambda^{\sigma_y}(y_o - \bar{y}) + \bar{y} \left[1 - \Lambda^{\sigma_y}(y_o - \bar{y}) \right] + \sigma_y^2 \cdot f^{\sigma_y}(y_o - \bar{y})$$

Resulting in the medium pressure solution:

$$\boxed{\bar{y} \approx \bar{y} + (y_o - \bar{y}) \Lambda^{\sigma_y}(y_o - \bar{y}) + \sigma_y^2 f^{\sigma_y}(y_o - \bar{y})} \quad (54)$$

Which is valid for $\bar{y} < 3\sigma_y + \delta_y$, but not for the lowest values of \bar{y} . This is caused by the fact that for $y < 0.211$ (see Appendix) $\beta(y)$ suddenly flattens out and almost becomes zero. The linear approximation does not hold for this situation

anymore, since the line crosses the y -axis at $y=1/4$, i.e. beyond the 0.211 point.

6.4 Amending the lowest \bar{y} values

Eq.54 represents an accurate solution for medium values of \bar{y} , but not for very low \bar{y} values, i.e. $\bar{y} < -2\sigma_y$ when $\Lambda(y_o - \bar{y}) \approx 1$ and $f(y_o - \bar{y}) \approx 0$ and Eq.54 yields that $\tilde{y} \approx y_o$. This is not correct, since in these circumstances \tilde{y} will be smaller y_o and should approach 0. Therefore a small correction has to be subtracted from Eq.54. This low \bar{y} or low-pressure correction can be expressed as:

$$y_o \cdot \Lambda^{\sigma_y}(y_o - \bar{y} - \delta_{lp}), \text{ where } \delta_{lp} \approx 2.7\sigma_y^* \quad (55)$$

The value of the shift δ_{lp} was chosen in such a way that the probability functions are roughly zero within the range of the bell curves. Note that $\bar{y} + \delta_{lp} \approx \bar{y} + 2.7\sigma_y$ is more or less the maximum value related to the bell curve centered around \bar{y} as can be seen in Fig.5.

Inclusion of this low pressure term into Eq.54 gives the following expression, valid for low- and medium \bar{y} -values:

$$\tilde{y} \approx \bar{y} + (y_o - \bar{y}) \Lambda^{\sigma_y}(y_o - \bar{y}) + \sigma_y^2 f^{\sigma_y}(y_o - \bar{y}) - \underbrace{y_o \cdot \Lambda^{\sigma_y}(y_o - \bar{y} - \delta_{lp})}_{\text{low } P \text{ correction}} \quad (56)$$

6.5 Amending the high \bar{y} values

Note that for larger values of \bar{y} , i.e. outside the low-to-medium pressure regime, $\Lambda(y_o - \bar{y}) \approx 0$ and $f(y_o - \bar{y}) \approx 0$ and Eq.56 yields that $\tilde{y} \rightarrow \bar{y}$. From the section 6.2 we know that due to the curvature of the $\beta(y)$ function, there is a small deviation, i.e. $\tilde{y} \approx \bar{y} + \delta_{hp}$ (Eq.42). This δ_{hp} shift is caused by the quadratic components in the β -function and is a consistent shift to the left away from \bar{y} . Fortunately it is possible to amend Eq.56 so that it also caters for the high pressure regime. This can be done in several ways, but the most elegant one is to replace \bar{y} in Eq.56 with its shifted equivalent $\bar{y} + \delta_{hp}$, where δ_{hp} is now defined by $-\Delta_{hp}/\bar{g}$ (see Eq.47), i.e. a function tapered in the low \bar{y} value regions as is reflected by the red curve in Fig.6. The result is:

* Note that $\bar{y} + \delta_{lp} \approx \bar{y} + 2.7\sigma_y$ is more or less the maximum value related to the bell curves displayed in Fig.5.

$$\begin{aligned} (\tilde{y} - \bar{y} - \delta_{hp}) &\approx (y_o - \bar{y} - \delta_{hp}) \Lambda^{\sigma_y}(y_o - \bar{y} - \delta_{hp}) \\ &\quad + \sigma_y^2 f^{\sigma_y}(y_o - \bar{y} - \delta_{hp}) \\ &\quad - y_o \cdot \Lambda^{\sigma_y}(y_o - \bar{y} - \delta_{hp} - \delta_{xx}) \end{aligned} \quad (57)$$

$$\text{where } \delta_{xx} = \delta_{lp} - \delta_{hp}$$

Eq.57 is a very symmetric expression[†] and applies to all valid values of \bar{y} , i.e. low, medium and high. It represents the solution of the upscaling problem in the y -space, i.e.

$$B_v^{up}(Q) = \bar{\phi} \exp\left(-\frac{1}{\bar{y}}\right)$$

However it still needs to be transformed back to the Q -domain.

7. Transformation back to the Q -domain

To express Eq.57 into the more familiar Q -domain parameters and thus the P_c parameters, the following substitutions are used (see also Eq.34):

$$\begin{aligned} u_o &= -\bar{g}(y_o - \bar{y} - \delta_{hp}) = Q_o - \bar{Q}_d - \Delta_{hp} \\ \tilde{u} &= -\bar{g}(\tilde{y} - \bar{y} - \delta_{hp}) = \tilde{Q}_d - \bar{Q}_d - \Delta_{hp} \end{aligned} \quad (58)$$

Plugging this into Eq.57 yields:

$$\frac{-1}{\bar{g}} \tilde{u} \approx \frac{-1}{\bar{g}} u_o \Lambda^{\sigma_y}\left(\frac{-1}{\bar{g}} u_o\right) + \sigma_y^2 f^{\sigma_y}\left(\frac{-1}{\bar{g}} u_o\right) - y_o \Lambda^{\sigma_y}\left(\frac{-1}{\bar{g}} u_o - \delta_{xx}\right)$$

which is equivalent to:

$$\tilde{u} \approx u_o \Lambda^{\sigma_y}\left(\frac{-1}{\bar{g}} u_o\right) - \bar{g} \sigma_y^2 f^{\sigma_y}\left(\frac{-1}{\bar{g}} u_o\right) + \frac{\bar{g}}{4} \Lambda^{\sigma_y}\left(\frac{-1}{\bar{g}} (u_o + \Delta_{xx})\right) \quad (59)$$

where $y_o = \frac{1}{4}$ and $\Delta_{xx} = \bar{g} \delta_{xx} = \bar{g}(\delta_{lp} - \delta_{hp}) = \Delta_{lp} + \Delta_{hp}$.

Here it should be noted that $\Delta_{lp} = \bar{g} \delta_{lp} \approx 2.7\sigma$ and is in general significantly larger than Δ_{hp} (see Eq.47 and Fig.7). Therefore it is safe to assume that $\Delta_{xx} = \Delta_{lp} + \Delta_{hp} \approx \Delta_{lp}$, i.e. the high-pressure shift has negligible effect on the low-pressure correction (as expected) and Eq.59 can thus be written as:

$$\tilde{u} \approx u_o \Lambda^{\sigma_y}\left(\frac{-1}{\bar{g}} u_o\right) - \bar{g} \sigma_y^2 f^{\sigma_y}\left(\frac{-1}{\bar{g}} u_o\right) + \frac{\bar{g}}{4} \Lambda^{\sigma_y}\left(\frac{-1}{\bar{g}} (u_o + \Delta_{lp})\right)$$

Using that $\Lambda^{\sigma_y}\left(\frac{1}{\bar{g}} x\right) = \Lambda^\sigma(x)$ and $\bar{g} \sigma_y^2 f^{\sigma_y}\left(\frac{1}{\bar{g}} x\right) = \sigma^2 f^\sigma(x)$ one gets:

$$\tilde{u} \approx u_o \Lambda^\sigma(-u_o) - \sigma^2 f^\sigma(-u_o) + \frac{\bar{g}}{4} \Lambda^\sigma[-(u_o + \Delta_{lp})]$$

Moreover, $\Lambda^\sigma(-x) = 1 - \Lambda^\sigma(x)$ and $f^\sigma(-x) = f^\sigma(x)$ and

[†] Disregarding the δ_{xx} shift in the low-pressure term.

\tilde{Q}_d builds up almost linearly until it reaches a level of just above the average value \bar{Q}_d . For high pressures, i.e. $Q > \bar{Q}_d + 3\sigma$ (about $Q > 4$ in Fig.8), $\rightarrow u_o \gg 0$ and $\Psi^\sigma(u_o) \approx f^\sigma(u_o) \approx \Psi^\sigma(u_o - \delta_{hp}) \approx 0$, i.e. $\tilde{u} \approx 0$ and thus $\tilde{Q}_d \approx \bar{Q}_d + \Delta_{hp}$, which slowly converges to \bar{Q}_d and for these higher pressures B_v^{up} can be expressed as:

$$B_v^{up}(Q) \approx \bar{\phi} \exp\left(\frac{-\bar{g}}{Q + \Delta_g - \bar{Q}_d + \Delta_{hp}}\right)$$

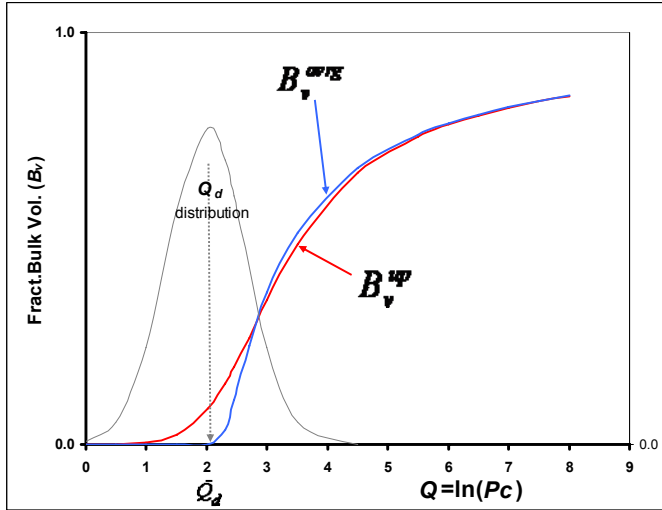


Fig.9: Comparing the upscaled fractional bulk volume B_v^{up} with the one non upscaled on based on the average Thomeer parameters. Please note that the average porosity is normalized, i.e. $\bar{\phi} = 1$. The Q_d distribution function is shown as well.

The resulting upscaled fractional bulk volume B_v^{up} of Eq.65 is shown in Fig.9. It is compared to the normal Bv for the average Thomeer parameters $\bar{\phi}$, \bar{g} and \bar{Q}_d , i.e.

$$B_v^{\bar{\phi}, \bar{g}, \bar{Q}_d}(Q) = \bar{\phi} \cdot \exp\left(\frac{-\bar{g}}{Q - \bar{Q}_d}\right) \quad (66)$$

The upscaled bulk volume shows that liquid intrusion happens much before the non upscaled one, where intrusion occurs above \bar{Q}_d . For Q's beyond the highest minimum entry pressures, i.e. $Q > \bar{Q}_d + 3\sigma$, the two curves overlap. This reflects the picture of the \tilde{Q}_d curve in Fig.8. It also indicates that for the B_v the small, g-upscaling induced, shift Δ_g has little effect.

Fig.10 is the more conventional display of the Bv curves of Fig.9, i.e. B_v versus P_c in a log-log display. The low pressure behavior of the upscaled function B_v^{up} is highlighted in this figure. The liquid intrusion for the large rock volumes happens at a much lower pressure than what can be expected from the average rock properties only. This means that in an oil reservoir there will be more oil present at the lower heights above the free water level. Than from single core plug data could be expected and modeled. For greater heights the upscaled and non upscaled curves more or less overlap.

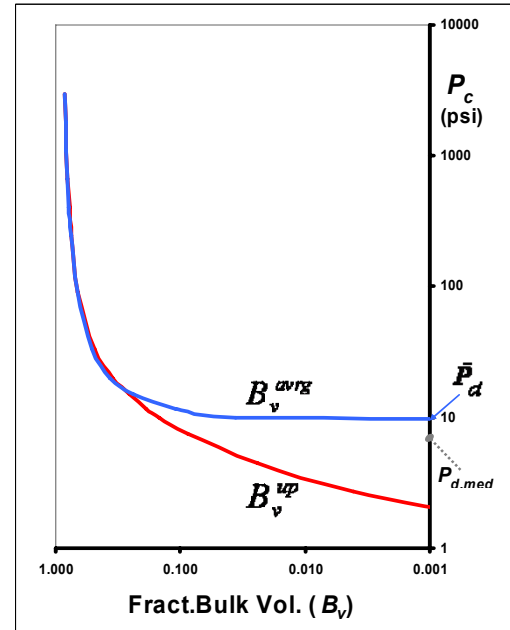
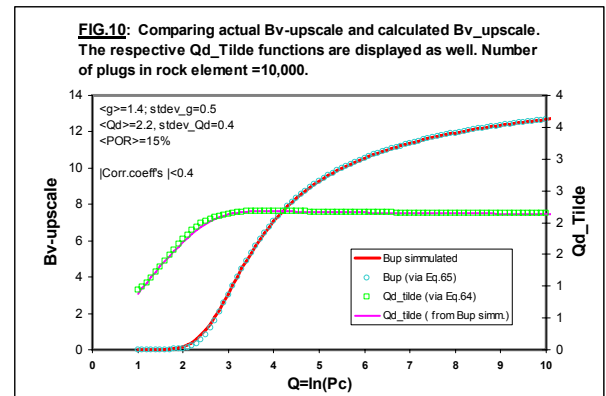


Fig.10: Comparison of the upscaled and average Fractional Bulk Volume Occupied (B_v) displayed in the more conventional way. In the low pressure regime, i.e. smaller than average $P_{d,med}$, the upscaled curve sets in at the lowest minimum entry pressure and increases almost linearly.

9. Comparison with Modeling

To assess the accuracy of the derived approximations (Eq.65 and 64) a rock element equivalent to 10,000 plugs was simulated.



The following parameters were used:

$$\bar{\phi} = 15\%;$$

$$\bar{G} = 0.6 \rightarrow \bar{g} = 2.3 \cdot \bar{G} = 1.38; \quad \sigma_G = 0.2 \rightarrow \sigma_g = 0.46$$

$$\bar{Q} = 2.2; \quad \sigma_{Q_d} \equiv \sigma = 0.4$$

Number of "plugs" = 10,000

$$|\text{Corr.Coeff}(\phi, g, Q_d)| < 0.4 \quad (\approx \text{negligible})$$

plug – plug correlation coeff. < 0.9 and has no effect.

The results are displayed in Fig.10. The difference between $B_{v,actual}^{up}$ and $B_{v,calculated}^{up}$ is small.

Conclusion

Here a direct and closed form approximation to the upscaling problem of mercury injection capillary pressure data to arbitrary large reservoir elements is presented. The method is based on standard Thomeer functions and a statistical consistent formalism has been derived based on Gaussian distributions of the key parameters.

The result retains the familiar form of the Thomeer function while replacing single plug values with statistical properties of these values within a petrophysical rock type. These results will now allow improved integration of core plug and log data processes for saturation-height function calibration to the remaining variables, i.e. subsurface wettability, reservoir fluid properties and electrical log interpretation parameters.

It is anticipated that statistically robust sample sets of MICP data within petrophysical rock types will become much more common for these purposes and progress will be accelerated in understanding subsurface fluid distributions, free-water level determinations and geometries, and that wettability references will improve reservoir analysis.

Nomenclature

MICP	Mercury Injection Capillary Pressure
P_c	Capillary pressure (applied Hg pressure) in psi
P_d	Minimum entry pressure in psi
$B_{v,\infty}$	Fract. Bulk Vol. occupied by Hg at $P_c=\infty$
B_v	Fract. Bulk Vol. occupied by Hg
$B_{v,i}$	Fract. Bulk Vol. occ. for core plug i
B_v^{ϕ,g,Q_d}	Fract. Bulk Vol. occ. For plug (ϕ, g, Q_d)
B_v^{up}	Upscaled Fract. Bulk Vol. occ. by Hg
b_g^{up}	Normalized F.B.V. occ. by Hg $B_v^{up} / \bar{\phi}$
$E[x]$	Expectation value of $x = \langle x \rangle$
G	Pore Geometrical Factor (PGF)
g	PGF in Q -domain of a core plug ($=2.3G$)
\bar{g}	Average of all g 's in the large rock
σ_g	Stand. deviation of the g 's.
σ	Stand. deviation of the Q_d 's.
Q	Applied Hg pressure in the Q -domain: $Q = \ln(P_c)$
Q_d	Minimum entry (Hg) pressure in the Q -domain
\bar{Q}_d	Average minimum entry pressure in the Q -domain
\tilde{Q}_d	Upscaled equivalent of \bar{Q}_d (not a constant)
\tilde{Q}_d	Preliminary notation ($=\tilde{Q}_d - \Delta_g$)
Δ_o	Shift in Q -domain caused by Q -integral
$Q_{d,o}$	Shifted min. entry pressure ($=Q - \Delta_o + \Delta_g$)
Ω	normalized distrib.func. in (ϕ, g, Q_d) space
ψ	normalized 1-D distribution functions
ϕ	porosity of a core plug
$\bar{\phi}$	average porosity of all plugs in a large rock element
$f_{\bar{x}}^\sigma(x)$	Normal distrib. (mean \bar{x} ; stand.dev. σ)

$\Lambda_{\bar{x}}^\sigma(x)$	Probability function (mean \bar{x} ; stand.dev. σ)
$\Psi_{\bar{x}}^\sigma(x)$	Complementary probability function
$\beta(y)$	intermediate function = $\exp(\frac{1}{y})$. See Appendix.
$\Delta_g \approx \frac{\sigma_g^2}{2\bar{g}}$	shift in Q -domain caused by variation in g (G).
Δ_{hp}	high pressure shift in Q -domain
$y = \frac{1}{\bar{g}}(Q + \Delta_g - Q_d)$	coordinate transformation from Q - to y -domain
$\bar{y} = \frac{1}{\bar{g}}(Q + \Delta_g - \bar{Q}_d)$	
$y_o = \frac{1}{\bar{g}}(Q + \Delta_g - Q_{d,o})$	
$\tilde{y} = \frac{1}{\bar{g}}(Q + \Delta_g - \tilde{Q}_d)$	
$u_o = Q_o - \bar{Q}_d - \Delta_{hp}$	intermediate coordinate transformation
$\tilde{u} = \tilde{Q}_d - \bar{Q}_d - \Delta_{hp}$	intermediate coordinate transformation
$\delta_y = \frac{\sigma_g^2}{2\bar{g}^2}$	- Shift in y -domain
δ_{hp}	- High pressure shift in y -domain
$\sigma_y = \frac{\sigma}{\bar{g}}$	- Standard deviation in y -domain

References

1. Thomeer, J.H.M., 1960, Introduction of a Pore Geometrical Factor Defined by a Capillary Pressure Curve, Petroleum Transactions, AIME, Vol 219, T.N. 2057, 354-358.
2. Ekran, S., 1999, Water Saturation Modeling: An Upscaling Point of View, SPE 56559.
3. Clerke, E.A., 2003, Beyond Porosity-Permeability Relationships – Determining Pore Network Parameters for the Ghawar Arab D using the Thomeer Method, GeoFrontier, Vol 1, Issue 3, September.
4. Clerke, E.A., Private communications, 2005

Acknowledgements

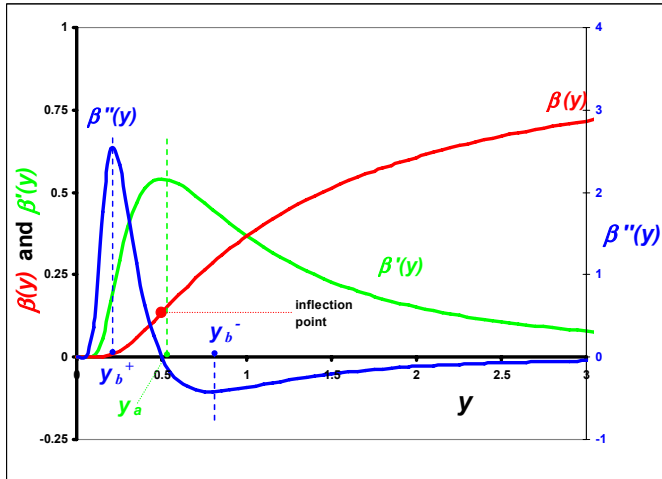
The author would like to acknowledge helpful discussions with Ed Clerke and Craig Phillips and he wishes to thank Saudi Aramco for allowing him to publish this work.

Appendix : Properties of the function $\beta(y)$

The exponential part of the Thomeer function in the Q -domain (see Eq.3) can be simplified by the β -function as introduced in section 6.1:

$$\beta(y) = \begin{cases} e^{-\frac{1}{y}} & \text{for } y > 0 \\ 0 & \text{for } y \leq 0 \end{cases}$$

The function is shown in the figure below and converges slowly to 1 for $y \rightarrow \infty$.



Derivatives:

$$\beta'(y) = \frac{\partial \beta}{\partial y} = \beta(y) \frac{1}{y^2}$$

$$\beta''(y) = \frac{\partial^2 \beta}{\partial y^2} = \beta(y) \frac{1}{y^3} \left(\frac{1}{y} - 2 \right)$$

$$\beta'''(\bar{y}) = \frac{\partial^3 \beta}{\partial y^3} = \beta(y) \frac{1}{y^4} \left(\frac{1}{y^2} - \frac{6}{y} + 6 \right)$$

Extremes:

First derivative

$$\beta'(y = y_a) \Rightarrow \beta''(y_a) = 0 \Rightarrow y_a = \frac{1}{2}$$

Point y_a corresponds also with the inflection point on the flank of the $\beta(y)$ function. Note that $\beta'(\frac{1}{2}) \approx 0.54$

Second derivative

$$\beta''(y = y_b) \Rightarrow \beta'''(y_b) = 0 \Rightarrow \frac{1}{y_b^2} - \frac{6}{y_b} + 6 = 0$$

Which has two solutions: $\begin{cases} y_b^+ = \frac{1}{3+\sqrt{3}} \approx 0.211 \\ y_b^- = \frac{1}{3-\sqrt{3}} \approx 0.789 \end{cases}$

y_b^+ corresponds to the point where the $\beta(y)$ function starts to grow, i.e. $\beta(0.211) \approx 0.009$ and $\beta(y < y_b^+) \approx 0$.

For low y 's $\beta(y)$ can be approximated by a tangent line through the inflection point, i.e.

$$\beta'(\frac{1}{2})(y - y_o)$$

This line crosses the y -axis at $y_o = 1/4$, see figure.

